Band and Vacancy Engineering in SnTe to Improve its Thermoelectric Performance

Zan Yang [a], *Evan Smith* [b], *Yu-Chih Tseng* [c], *Kamil Ciesielski* [d], *Sergei Novikov* [a], *Thomas Kalab* [a], *Yuyang Huang*[a], *Eric Toberer* [d] *and Yurij Mozharivskyj** [a]

* **Corresponding Author**

[a] Department of Chemistry and Chemical Biology, McMaster University, Ontario, Canada.

[b] Department of Physics and Astronomy, McMaster University, Ontario, Canada.

[c] CanmetMATERIALS, Natural Resources Canada, Ontario, Canada.

[d] Physics Department, Colorado School of Mines, America.

Temperature-Dependent Single Kane Band Model

Because of the narrow band gap (0.18 eV at room temperature), the L band strongly interacts with the conduction band, making it highly non-parabolic. Therefore, the L band is considered as a Kane band. By applying the single Kane band model to the L band, we have[1]

$$S = \frac{k_B}{e}\left[\frac{{}^{1}F_{-2}^{1}}{{}^{0}F_{-2}^{1}} - \xi\right] \tag{S1}$$

$$L = \left(\frac{k_B}{e}\right)^2\left[\frac{{}^{2}F_{-2}^{1}}{{}^{0}F_{-2}^{1}} - \left(\frac{{}^{1}F_{-2}^{1}}{{}^{0}F_{-2}^{1}}\right)^2\right] \tag{S2}$$

$$p = Ap_{Hall} = \frac{\left(2m_d^* k_B T\right)^{3/2}}{3\pi^2\hbar^3}{}^{0}F_{0}^{3/2} \tag{S3}$$

$$A = \frac{3K(K+2)\,{}^{0}F_{-4}^{1/2}\,{}^{0}F_{0}^{3/2}}{(2K+1)^2\,\left({}^{0}F_{-2}^{1}\right)^2} \tag{S4}$$

$${}^{n}F_{k}^{m} = \int_0^\infty \left(-\frac{\partial f}{\partial \varepsilon}\right)\varepsilon^n\left(\varepsilon+\alpha\varepsilon^2\right)^m\left[(1+2\alpha\varepsilon)^2+2\right]^{k/2}d\varepsilon \tag{S5}$$

Where k_B is the Boltzmann constant, ξ is the reduced Fermi energy $\xi = E_f/k_BT$. $\hbar$ is the reduced Plank's constant, m_d^* is the DOS effective mass of the L band, S and L are the Seebeck coefficient and Lorenz number, respectively. p is the carrier concentration, p_{Hall} is the Hall carrier concentration, A is the Hall factor, μ_{Hall} is the Hall mobility, τ_{total} is the total relaxation time, and

${}^{n}F_{k}^{m}$ is the Fermi integration. α is the non-parabolic parameter, $\alpha = {k_B T}/{E_g}$, and ε is the reduced energy, $\varepsilon = {E}/{k_B T}$. $K = m_{\perp}^{*} / m_{\parallel}^{*}$ where $m_{\perp}^{*}$ and $m_{\parallel}^{*}$ are the transverse and longitudinal effective mass, respectively. For SnTe, $K = 4$[2].

$$m_I^* = 3\left(\frac{2}{m_{\perp}^*} + \frac{1}{m_{\parallel}^*}\right)^{-1} \tag{S6}$$

$$m_L^* = N_V^{2/3} m_b^* = N_V^{2/3}\left(m_{\perp}^{*\,2} m_{\parallel}^*\right)^{1/3} \tag{S7}$$

m_I^* and m_L^* are the inertia and DOS effective mass of the L band, respectively. N_v is the band degeneracy of L band, $N_v = 4$. It is well known that the band morphology of SnTe varies strongly with temperature, which makes the DOS effective mass temperature dependent. Therefore, to improve the accuracy of the simulation, we considered the temperature dependency of the band gap by introducing the Varshni model[3]:

$$E_g = E_g(0) - \frac{CT^2}{T + D} \tag{S8}$$

Here E_g (0) = 0.25eV is the band gap at 0K, C and D are the fitting parameters. Based on the simulation of Jose et al.'s work[4], C and D are determined to be 2.078×10^{-4} eV/K and -8.673×10^{-4} K, respectively.

Temperature-Dependent Two Band Model

It is well known that the band morphology of SnTe varies strongly with temperature, which results in fluctuations of the DOS effective mass. To improve the accuracy of the simulation, we considered the temperature dependency of the band gap by introducing the Varshni model[3] into the well-established two-band model of SnTe[5]. We also allowed the DOS effective masses of the L and Σ bands, as well as $\Delta E_{L\text{-}\Sigma}$, to vary with temperature. The weighted combination of two bands gives the total Seebeck coefficient and Lorenz number of the system[6]

$$S_{total} = \frac{S_L p_{N,L} b + S_H p_{N,H}}{p_{N,L} b + p_{N,H}} \tag{S9}$$

$$L_{total} = \frac{L_L p_{N,L} b + L_H p_{N,H}}{p_{N,L} b + p_{N,H}} \tag{S10}$$

Where S_L and S_H, L_L and L_H, σ_L and σ_H, μ_L, and μ_H are the Seebeck coefficient, Lorenz number, electrical conductivity and mobility of the light hole band (L) and heavy hole band (Σ),

respectively. The paramter $b = \mu_L/\mu_H$, and it is set to 8 for SnTe[7]. Because of the narrow band gap (0.18 eV at room temperature), the L band strongly interacts with the conduction band, making it highly non-parabolic. Therefore, the L band is considered a Kane band. By applying the Kane band model to the L band, we have[1]

$$S_L = \frac{k_B}{e}\left[\frac{{}^1F_{-2}^{\ 1}}{{}^0F_{-2}^{\ 1}} - \xi\right] \tag{S11}$$

$$L_L = \left(\frac{k_B}{e}\right)^2\left[\frac{{}^2F_{-2}^{\ 1}}{{}^0F_{-2}^{\ 1}} - \left(\frac{{}^1F_{-2}^{\ 1}}{{}^0F_{-2}^{\ 1}}\right)^2\right] \tag{S12}$$

$$p_L = \frac{\left(2m_L^* k_B T\right)^{3/2}}{3\pi^2\hbar^3}\,{}^0F_0^{3/2} \tag{S13}$$

$$A_L = \frac{3K(K+2)\,{}^0F_{-4}^{1/2}\,{}^0F_0^{3/2}}{(2K+1)^2\ \left({}^0F_{-2}^{\ 1}\right)^2} \tag{S14}$$

m_L^* is the DOS effective mass of the L band and A_L is the Hall factor of the L band.

For the heavy hole Σ band, because of the significant energy separation with the L band (~ 0.3 eV), it is assumed that its interaction with the conduction band is small enough to be considered a parabolic band. Therefore, we use the parabolic band model to simulate the contribution from the Σ band[8]

$$S_\Sigma = \frac{k_B}{e}\left[\frac{2F_1}{F_0} - (\xi - \Delta)\right] \tag{S15}$$

$$L_\Sigma = \left(\frac{k_B}{e}\right)^2\left[\frac{3F_2(\xi)}{F_1(\xi)} - \left[\frac{2F_1(\xi)}{F_0(\xi)}\right]^2\right] \tag{S16}$$

$$p_\Sigma = \frac{\left(2m_H^* k_B T\right)^{3/2}}{3\pi^2\hbar^3}\,\frac{2F_0^2(\xi)}{F_{-1/2}(\xi)} \tag{S17}$$

$$A_\Sigma = \frac{3}{2}F_{1/2}\frac{F_{-1/2}}{2F_0^2} \tag{S18}$$

$$F_s = \int_0^\infty \frac{\varepsilon^s}{1 + exp(\varepsilon - \xi - \Delta)}d\varepsilon \tag{S19}$$

Where F_s is the Fermi integration of the parabolic condition, $m_{d,L}^*$ is the DOS effective mass of the

heavy hole Σ band, and Δ is the reduced energy separation between the L and Σ bands, $\Delta = \Delta E_{L-\Sigma}/k_B T$. Here, $d\Delta E_{L-\Sigma}/dT$ is taken as 0.0003eV/K and the value of m_H^* is directly fitted according to the simulation results given by Zhou et al. [5].

Doping Effect of Ge in SnTe

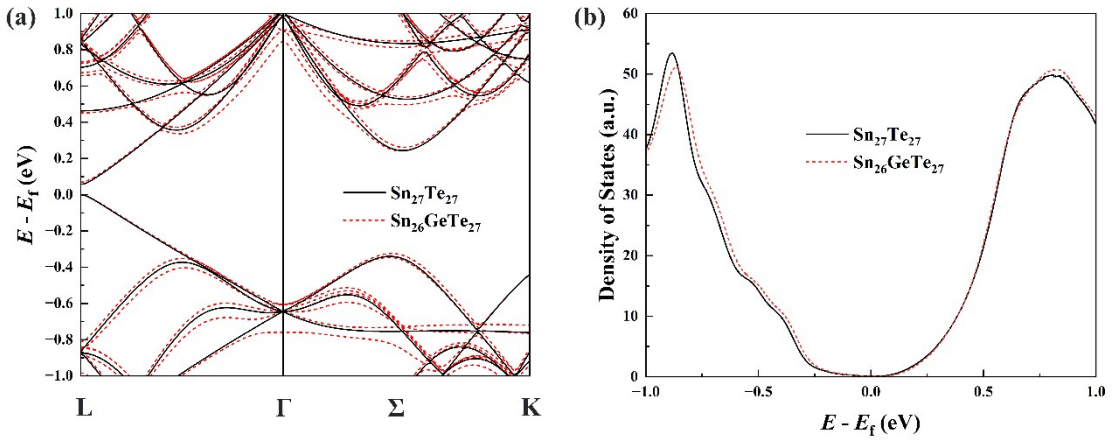

Figure S1. Doping effect of Ge in SnTe. (a) Band structure and (b) density of states. The solid black line and red dashed line represent the pristine SnTe and Ge-doped SnTe, respectively.

Single and Multi-Band Model Simulation Results

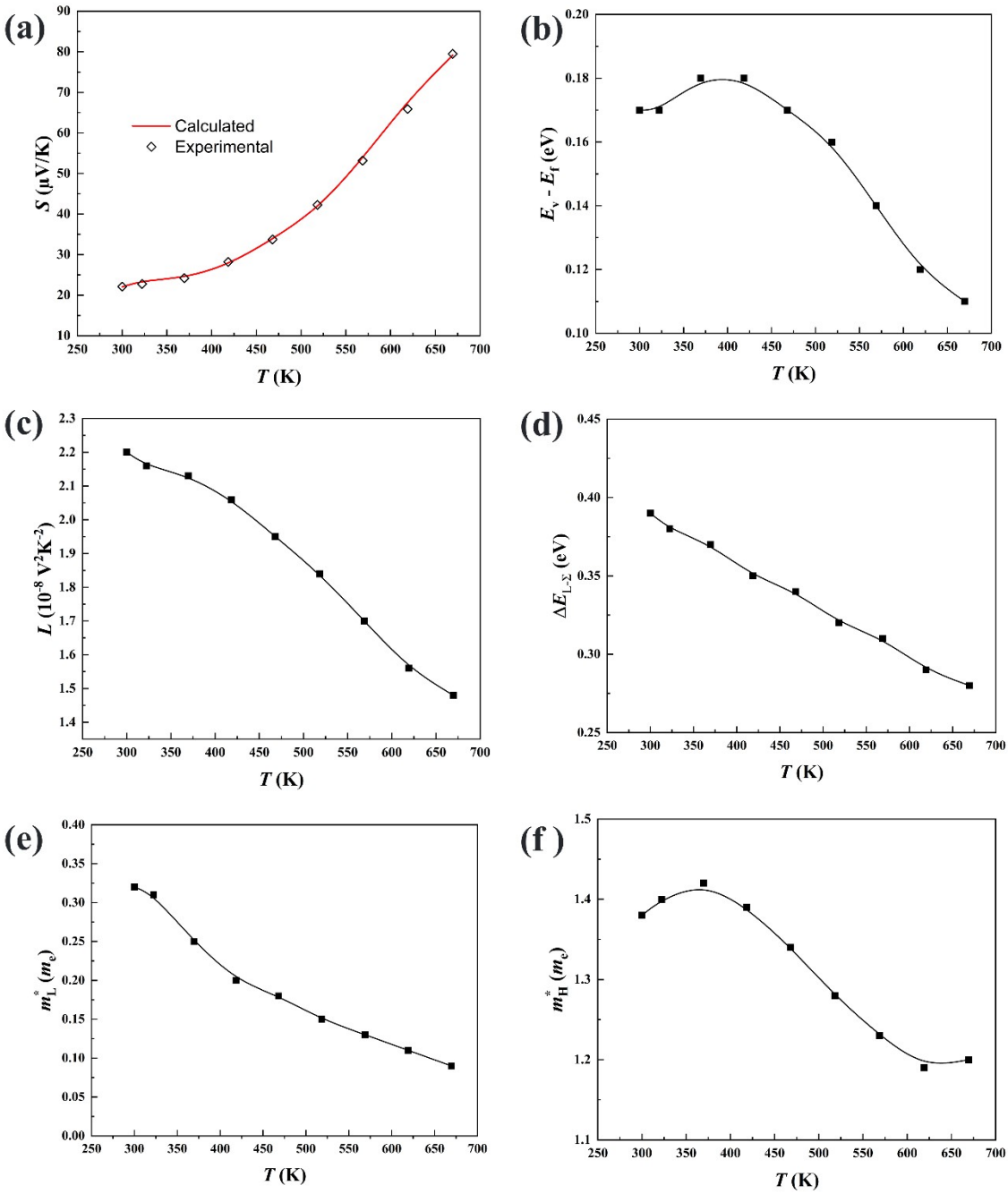

Figure S2. TD-TB simulation results for $Sn_{0.98}Ge_{0.05}Te$. (a) Seebeck coefficient, (b) energy separation between top of the valence band E_V and Fermi level E_f, (c) Lorenz number, (d) Energy separation between the L and Σ bands, (e) DOS effective mass of the L band, and (f) DOS effective mass of the Σ band. The black lines in (b) ~ (f) are guide for the eyes.

As shown in **Figure S3** (a), most of the carriers are located at the L band, which suggests the

contribution of the lower Σ band may be neglectable. This can be verified by comparing the Lorenz numbers calculated by the two-band model and single-band model shown in **Figure S3** (b). The simulation result shows that the Σ band has very little impact on the outcome. Therefore, for simplicity, we used the single band model to calculate the Lorenz number for all samples.

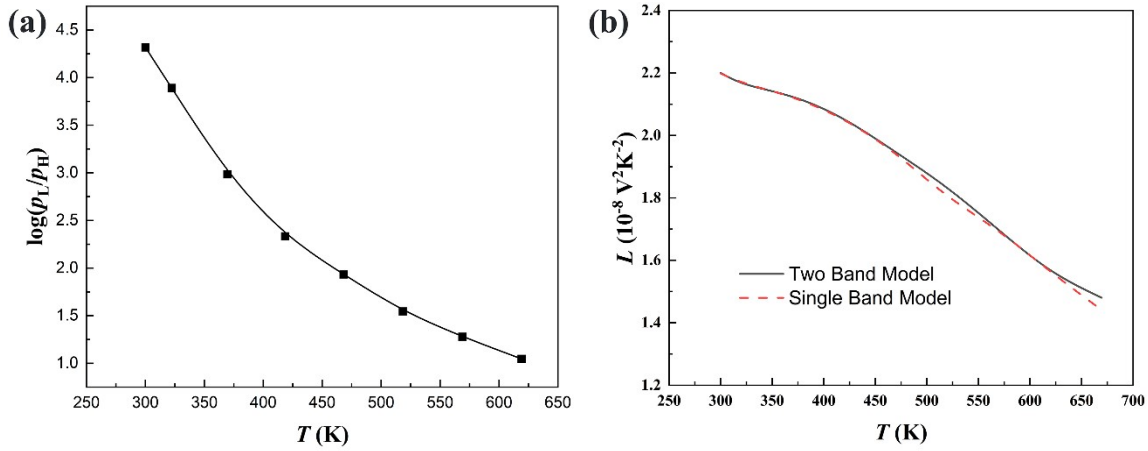

Figure S3. (a) The natural logarithm of the ratio of carrier concentrations distributed in the L and Σ bands. (b) Lorenz number computed by the two-band model (solid black line) and single-band model (red dash line).

Scattering Factor Determination

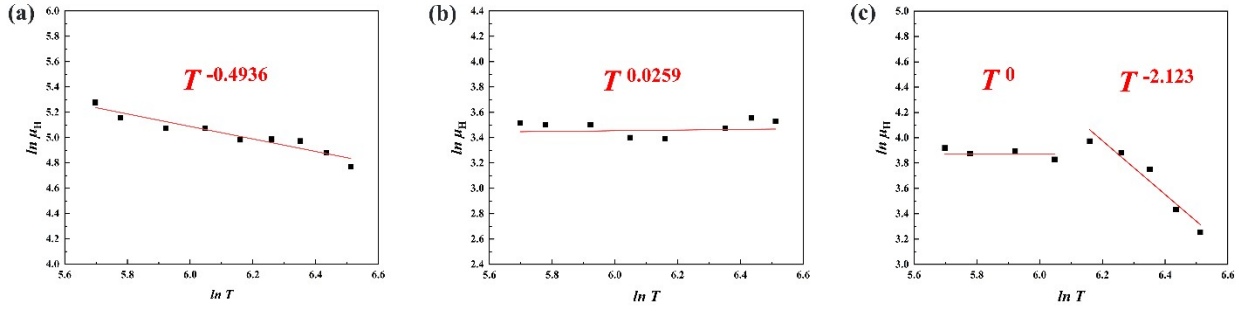

Figure S4. $\ln \mu_H$ vs. $\ln T$ of $(Sn_{0.98}Ge_{0.05}Te)_{1-x}(Sb_2Pb_yTe_3)_x$ series. (a) $x = 0$, $y = 0$, (b) $x = 0.09$, $y = 0$ and (c) $x = 0.09$, $y = 0.5$ (see main text).

Electron Backscatter Diffraction Analysis

From our electron backscatter diffraction analysis, we find that Pb compensation increases the average grain size from 0.6 μm to 1.36 μm. $SnTe_3O_8$ (yellow area in phase maps of Figure S5 (c), (d)) could be found along the grain boundaries, which is caused by the inevitable oxidation during the sample synthesis.

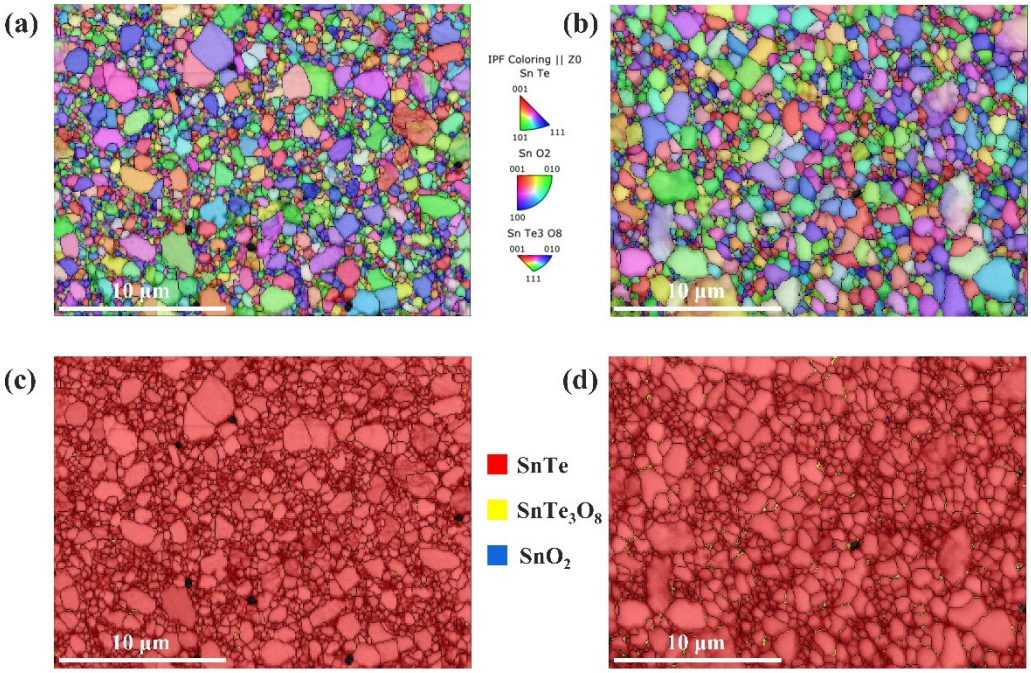

Figure S5. (a), (c) Electron backscatter diffraction map and phase map of $(Sn_{0.98}Ge_{0.05}Te)_{0.91}(Sb_2Te_3)_{0.09}$ and (b), (d) electron backscatter diffraction map and phase map of $(Sn_{0.98}Ge_{0.05}Te)_{0.91}(Sb_2Pb_{0.5}Te_3)_{0.09}$.

Effect of Sb Precipitation

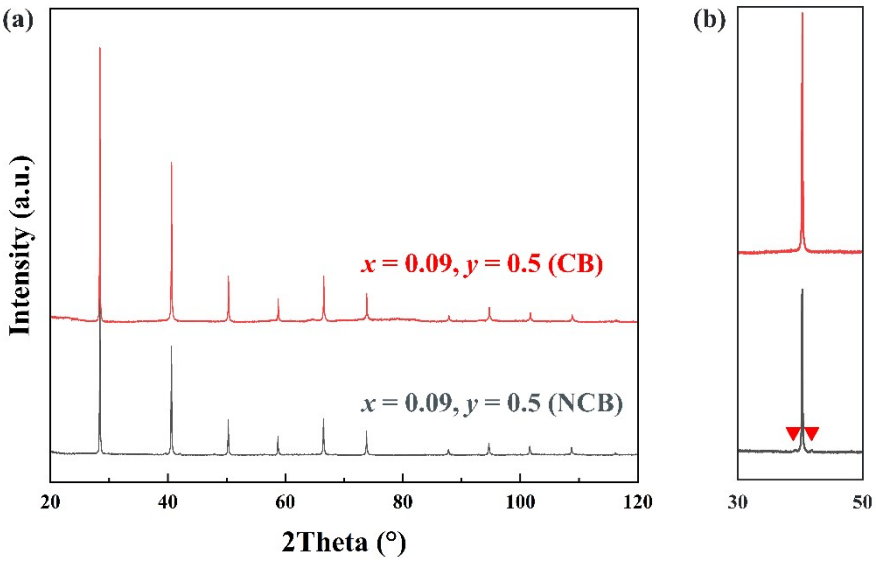

Figure S6. (a) Powder XRD pattern of the NCB and CB samples (see main text). (b) A close-up image of the pattern in the range from 30° to 50°; the peaks marked by red triangles result from Sb precipitates.

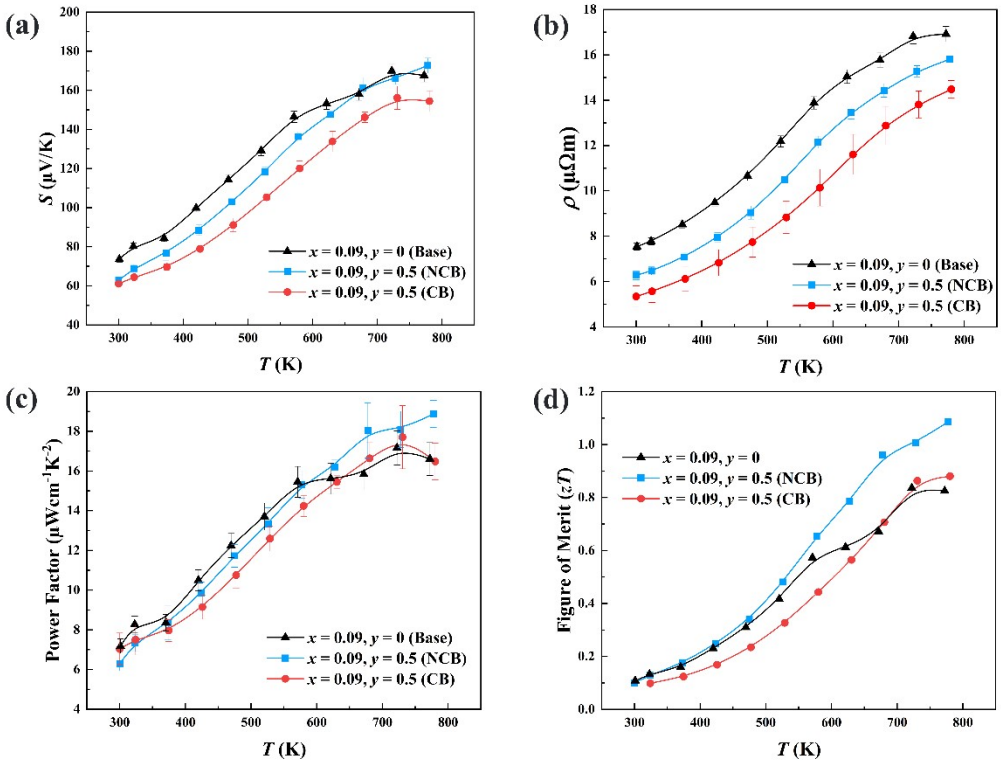

Figure S7. A comparison of (a) Seebeck coefficient, (b) resistivity, (c) power factor and (d) zT values between Base, CB and NCB samples (see main text).

The compositions of base material (Base), charge balanced (CB) sample and the non-charge balanced (NCB) sample are $(Sn_{0.98}Ge_{0.05}Te)_{0.91}(Sb_2Te_3)_{0.09}$, $(Sn_{0.98}Ge_{0.05}Te)_{0.91}(Sb_{1.4644}Pb_{0.5}Te_3)_{0.09}$ and $(Sn_{0.98}Ge_{0.05}Te)_{0.91}(Sb_2Pb_{0.5}Te_3)_{0.09}$, respectively.

Reproducibility Test

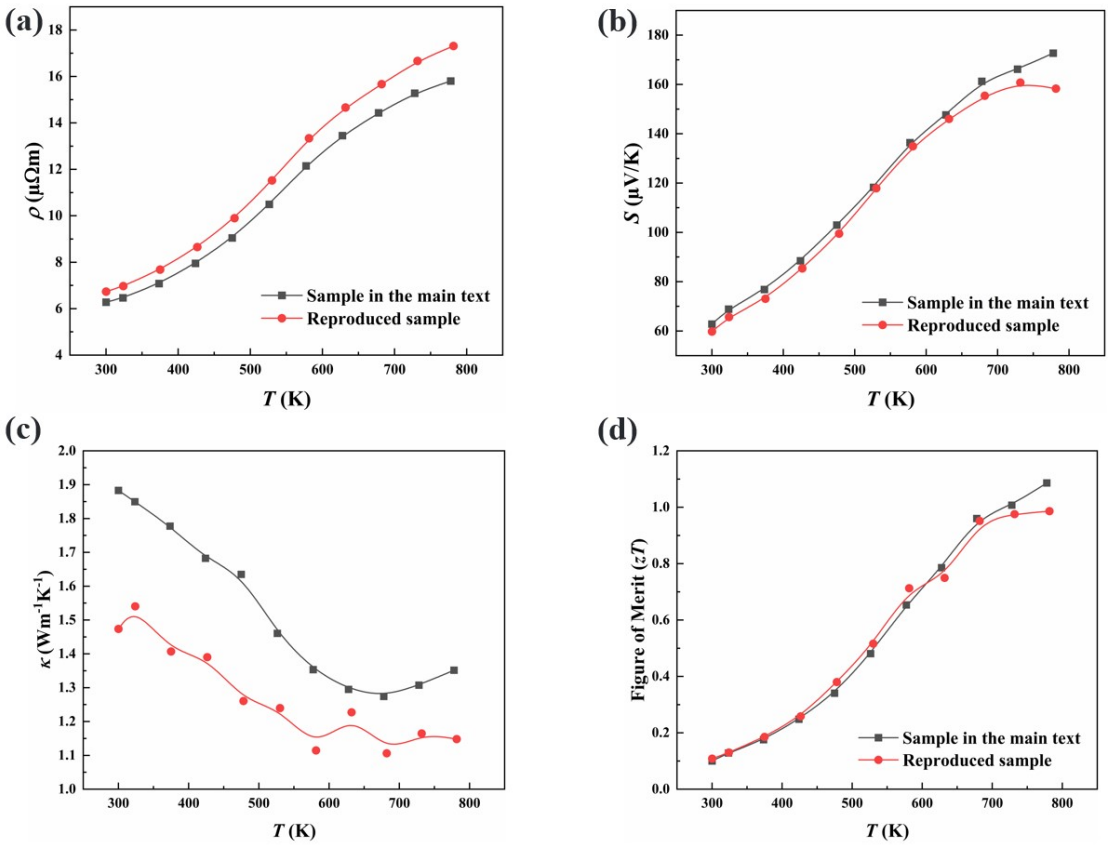

Figure S8. (a) Electrical resistivity, (b) Seebeck coefficient, (c) thermal conductivity and (d) zT value of three trials. Samples of these trials are synthesised separately using the same method.

Table S1. Density of Samples

Composition	ρ_M (gcm^{-3})	ρ_T (gcm^{-3})	Relative Density (%)
$x = 0, y = 0$	6.16	6.41	96.10
$x = 0.03, y = 0$	6.33	6.43	98.44
$x = 0.06, y = 0$	6.16	6.30	97.78
$x = 0.09, y = 0$	6.09	6.34	96.06
$x = 0.09, y = 0.2$	6.14	6.40	95.94
$x = 0.09, y = 0.5$	6.36	6.53	97.40
$x = 0.09, y = 0.8$	6.31	6.62	95.32

Table S2. Room-Temperature Hall Data

Composition	p_{Hall} (10^{20} cm^{-3})	μ_{Hall} (cm^{2}V^{-1}s^{-1})	m_L^* (m_e)
$x = 0$, $y = 0$	1.89	195.91	0.32
$x = 0.03$, $y = 0$	2.87	64.11	0.79
$x = 0.06$, $y = 0$	2.87	45.51	0.87
$x = 0.09$, $y = 0$	2.60	33.40	1.04
$x = 0.09$, $y = 0.2$	2.56	41.83	0.91
$x = 0.09$, $y = 0.5$	2.10	50.42	0.80
$x = 0.09$, $y = 0.8$	1.87	56.38	0.74

Table S3. Selected crystallographic data, experimental details, and refinement results for the $(Sn_{0.98}Ge_{0.05}Te)_{1-x}(Sb_2Pb_yTe_3)_x$ single crystals.

Composition	$x = 0$ $y = 0$	$x = 0.03$ $y = 0$	$x = 0.06$ $y = 0$	$x = 0.09$ $y = 0$	$x = 0.09$ $y = 0.2$	$x = 0.09$ $y = 0.5$	$x = 0.09$ $y = 0.8$
Sn Site Occupancy (%)	97.7(2)	95.7(5)	94.3(4)	92.9(1)	94.1(5)	95.1(3)	97.6(3)
Crystal System	Cubic						
Space Group	$Fm\bar{3}m$						
***a*, Å**	6.3030(7)	6.2879(7)	6.2775(7)	6.2672(7)	6.2751(7)	6.2756(7)	6.2858(7)
***Volume*, Å^3**	250.40(8)	248.61(8)	247.38(8)	246.16(8)	247.09(8)	247.15(8)	248.36(8)
Z	4						
μ/mm^{-1}	20.978	20.933	20.889	20.868	20.987	20.908	21.175
***F*(000)**	404	400	396	394	398	396	404
***2Θ* Range (°)**	5.604 - 34.319	5.618- 34.413	5.627- 34.478	5.636- 32.135	5.629- 34.493	5.629- 34.490	5.619- 32.029
Index Ranges	$-10 \le h \le 10$ $-10 \le k \le 9$ $-10 \le l \le 10$	$-10 \le h \le 10$ $-9 \le k \le 10$ $-10 \le l \le 10$	$-10 \le h \le 10$ $-9 \le k \le 10$ $-10 \le l \le 9$	$-9 \le h \le 8$ $-9 \le k \le 9$ $-9 \le l \le 9$	$-10 \le h \le 9$ $-10 \le k \le 10$ $-8 \le l \le 10$	$-10 \le h \le 9$ $-10 \le k \le 9$ $-10 \le l \le 7$	$-9 \le h \le 9$ $-8 \le k \le 9$ $-7 \le l \le 9$
Reflections Collected	1587	1110	1102	1387	1095	1070	567
Data/Restraints/ Parameters	46/0/4	46/0/5	46/0/4	39/0/4	46/0/5	46/0/4	38/0/4
GOOF	1.240	1.067	0.937	0.908	1.193	1.293	1.139
R_1 (I>2σ (I))	0.0130	0.0109	0.0141	0.0052	0.0107	0.0258	0.0110
Largest diff. peak/hole (e/Å^3)	0.660/-0.642	0.559/-0.242	0.380/-0.434	0.357/-0.212	0.51/-0.61	0.88/-1.36	0.36/-0.70

Table S4. Sound Velocity Measurement data. v_l is the longitudinal velocity, v_t is the transverse velocity, and v is the bulk sound velocity.

Composition	v_l (m/s)	v_t (m/s)	v (m/s)
$x = 0, y = 0$	3300.8	1911.7	2121.8
$x = 0.03, y = 0$	3293.8	1898.2	2107.7
$x = 0.06, y = 0$	3201.2	1836.7	2040.2
$x = 0.09, y = 0$	2863.2	1694.0	1876.5
$x = 0.09, y = 0.2$	3191.7	1825.5	2028.3
$x = 0.09, y = 0.5$	3183.0	1841.7	2044.2
$x = 0.09, y = 0.8$	2927.3	1698.5	1884.8

Here v is given by

$$v = \left[\frac{1}{3}\left(\frac{1}{v_l^3} + \frac{2}{v_t^3}\right)\right]^{-1/3} \tag{S20}$$

References

(1) Pei, Y.; LaLonde, A. D.; Wang, H.; Snyder, G. J. Low Effective Mass Leading to High Thermoelectric Performance. *Energy Environ. Sci.* **2012**, *5* (7), 7963. https://doi.org/10.1039/c2ee21536e.

(2) Seddon, T.; Gupta, S. C.; Saunders, G. A. Hole Contribution to the Elastic Constants of SnTe. *Solid State Communications* **1976**, *20* (1), 69–72. https://doi.org/10.1016/0038-1098(76)91701-4.

(3) Varshni, Y. P. TEMPERATURE DEPENDENCE OF THE ENERGY GAP IN SEMICONDUCTORS. 6.

(4) Querales-Flores, J. D.; Aguado-Puente, P.; Dangić, Đ.; Cao, J.; Chudzinski, P.; Todorov, T. N.; Grüning, M.; Fahy, S.; Savić, I. Towards Temperature-Induced Topological Phase Transition in SnTe: A First-Principles Study. *Phys. Rev. B* **2020**, *101* (23), 235206. https://doi.org/10.1103/PhysRevB.101.235206.

(5) Zhou, M.; Gibbs, Z. M.; Wang, H.; Han, Y.; Xin, C.; Li, L.; Snyder, G. J. Optimization of Thermoelectric Efficiency in SnTe: The Case for the Light Band. *Phys. Chem. Chem. Phys.* **2014**, *16* (38), 20741–20748. https://doi.org/10.1039/C4CP02091J.

(6) Lundstrom, M. S.; Jeong, C. *Near-Equilibrium Transport: Fundamentals and Applications*; World Scientific Publishing Company, 2012; Vol. 2.

(7) Rogers, L. M. Valence Band Structure of SnTe. *J. Phys. D: Appl. Phys.* **1968**, *1* (7), 845–852. https://doi.org/10.1088/0022-3727/1/7/304.

(8) May, A. F.; Snyder, G. J. Introduction to Modeling Thermoelectric Transport at High Temperatures.